Draft version July 27, 2010
Preprint typeset using LaTeX style emulateapj v. 5/25/10

EXTENDED X-RAY EMISSION IN THE HI CAVITY OF NGC 4151: GALAXY-SCALE AGN FEEDBACK?

Junfeng Wang[1], Giuseppina Fabbiano[1], Guido Risaliti[1,2], Martin Elvis[1], Carole G. Mundell[3], Gaelle Dumas[4], Eva Schinnerer[4], and Andreas Zezas[1,5]

Draft version July 27, 2010

ABSTRACT

We present the *Chandra* discovery of soft diffuse X-ray emission in NGC 4151 ($L_{0.5-2keV} \sim 10^{39}$ erg s^{-1}), extending $\sim$2 kpc from the active nucleus and filling in the cavity of the HI material. The best fit to the X-ray spectrum requires either a $kT \sim 0.25$ keV thermal plasma or a photoionized component. In the thermal scenario, hot gas heated by the nuclear outflow would be confined by the thermal pressure of the HI gas and the dynamic pressure of inflowing neutral material in the galactic disk. In the case of photoionization, the nucleus must have experienced an Eddington limit outburst. For both scenarios, the AGN-host interaction in NGC 4151 must have occured relatively recently (some 10^4 yr ago). This very short timescale to the last episode of high activity phase may imply such outbursts occupy $\gtrsim$1% of AGN lifetime.

Subject headings: X-rays: galaxies — galaxies: Seyfert — galaxies: jets — galaxies: individual (NGC 4151)

1. INTRODUCTION

NGC 4151 ($D \sim 13.3$ Mpc, $1'' = 65$ pc; Mundell et al. 1999) is often considered the nearest and apparently brightest archetypal Seyfert 1 galaxy (see Ulrich 2000 for a review). Extensively observed across the electromagnetic spectrum, it thus offers one of the best chances of studying the interaction between an active galactic nucleus (AGN) and the interstellar medium (ISM) in the galactic disk of its host. Such interaction, or "feedback", is recognized to play a key role in the supermassive black hole (SMBH) and host galaxy coevolution (e.g., Silk & Rees 1998). Direct observational constraints are still lacking on how efficient the AGN outflows are at depositing their energy in the host ISM (e.g., Hopkins & Elvis 2010; Ostriker et al. 2010).

NGC 4151 has a biconical extended narrow line region (ENLR) aligned along the Northeast–Southwest direction (P.A.$\sim$65°/230°; e.g., Evans et al. 1993; Kaiser et al. 2000), which shows extended soft X-ray emission in the central 10″ region (e.g., Elvis et al. 1983; Ogle et al. 2000; Yang et al. 2001; González-Martín 2008). Published work on imaging the circum-nuclear region of NGC 4151 has explored features on a few 10 pc to $\sim$1 kpc from the nucleus (e.g., Pedlar et al. 1992; Mundell et al. 1995; Asif et al. 1998; Mundell et al. 2003; Das et al. 2005; Kraemer et al. 2008; Wang et al. 2009; Storchi-Bergmann et al. 2009, 2010).

In this Letter, we present the discovery of soft diffuse X-ray emission extending $\gtrsim$2 kpc from the active nucleus and we discuss its implications.

[1] Harvard-Smithsonian Center for Astrophysics, 60 Garden St, Cambridge, MA 02138
[2] INAF-Arcetri Observatory, Largo E, Fermi 5, I-50125 Firenze, Italy
[3] Astrophysics Research Institute, Liverpool John Moores University, Birkenhead CH41 1LD, UK
[4] Max-Planck-Institut für Astronomie, Königstuhl 17, D-69117 Heidelberg, Germany
[5] Physics Department, University of Crete, P.O. Box 2208, GR-710 03, Heraklion, Crete, Greece

2. OBSERVATIONS AND REDUCTION

NGC 4151 was observed by *Chandra* with ACIS-S (Garmire et al. 2000) in 1/8 sub-array mode during March 27-29, 2008. The nucleus was placed near the aimpoint on the S3 chip. The data were reprocessed and analyzed following the standard procedures[6] using CIAO (Version 4.2) and CALDB (Version 4.2.0). After removing brief times of high background count rates, the cleaned data have total good exposure times of 116 ks and 63 ks, in ObsID 9217 and ObsID 9218 respectively.

The two ACIS observations of NGC 4151 were then merged to create a single event file. The ACIS readout streaks along P.A.= 174°/354° were removed with CIAO tool *acisreadcorr*[7]. Point source detection was done with *wavdetect* (Freeman et al. 2002) and 24 sources were removed from the images. We extracted the soft-band (0.3–1 keV) image and applied adaptive smoothing using CIAO tool *csmooth*, with a minimum significance 3σ. The same smoothing kernel was applied to the exposure map, which was then divided to get the exposure corrected image.

3. RESULTS

3.1. *Multiwavelength Morphology*

Figure 1a shows the resulting soft X-ray image ($3' \times 3'$, $\sim$12 kpc on a side). Note that the non-detection of X-ray emission towards the northernmost and southernmost part of the image is artificial, because this area is out of the ACIS-S field of view (FOV) for our observation (Figure 1a). Figure 1b presents a composite image of the same region in NGC 4151, consisting of soft X-ray (0.3–1 keV), exposure corrected *Chandra* ACIS image (blue), with the HI λ21 cm map (red) and a continuum-subtracted Hα image (green; Knapen et al. 2004).

The kpc-scale HI distribution (Mundell & Shone 1999) appears as a ring with brightest emission in the NW and SE (white contours in Figure 1a). The VLA fluxes

[6] `http://cxc.harvard.edu/ciao/threads/createL2/`
[7] `http://cxc.harvard.edu/ciao/ahelp/acisreadcorr.html`

(Mundell et al. 1999) agree well with lower resolution single dish measurements (Pedlar et al. 1992), supporting that the apparent central cavity is truly devoid of HI. Towards the nuclear region, only localized HI absorption toward the radio jet is found (Mundell et al. 1995, 1999). Inside this oval HI distribution, CO line emission (Dumas et al. 2010) is prominent in two lanes ∼1 kpc north and south of the nucleus (red contours in Figure 1a), and coincident with the circum-nuclear dust ring (Asif et al. 1998).

The ionized gas traced by Hα is mainly located in the ∼20″-long biconical ENLR (cyan=Hα+X-ray in Figure 1b) along the NE-SW direction centered on the nucleus, which closely follows the high excitation emission line gas (e.g., [OIII]5007, Kaiser et al. 2000; magenta contours in Figure 1a) photoionized by the AGN radiation. There is also Hα emission associated with a string of HII regions located along the NW and SE edges of the large-scale stellar bar (yellow=Hα+HI; Pérez-Fournon & Wilson 1990).

The soft X-ray emission is brightest in the nuclear region and central 15″, extending along the same direction as the ENLR bicone (P.A.∼65°/230°; appearing as the cyan rectangle in Figure 1b). This emission and the associated morphological features will be discussed in detail in a companion paper (Wang et al., in preparation).

Two X-ray clumps are present at the terminals of the bicone (marked as "interaction" in Figure 1b), where the outflows appear to encounter dense materials (CO gas lane in the NE and HI clump in the SW). In addition, there are two regions of X-ray enhancements in the HI ring (marked as "HII" in Figure 1b), spatially coincident with known HII regions (Pérez-Fournon & Wilson 1990). There are also some anti-correlations in the spatial distribution of X-ray emission relative to the HI material due to obscuration of the soft X-rays. Beyond the HI material (∼60″ from the nucleus), the X-ray emission becomes weak to the east and absent to the west.

Here we focus on the presence of the previously unknown, faint soft X-ray emission, which is seen extending beyond a radius of 30″ (∼2 kpc), filling the cavity in the HI distribution.

3.2. *Characterizing the Soft X-ray Emission*

We extracted X-ray data from an elliptical region centered at the nucleus (yellow polygon in Figure 1a), which covers the HI cavity and excludes the inner brighter emission ($r \lesssim 15''$) associated with the nucleus and the optical outflow. We measured the background level to be 0.050±0.006 counts per ACIS pixel, selecting alternative background regions in the image $2' - 3'$ away from NGC 4151. We find that the extended emission (0.3–1 keV) in the cavity region is significant (1562 counts vs. 728 counts expected from background) at 11σ ($F_{0.5-2keV} = 3.2 \times 10^{-14}$ erg s^{-1} cm^{-2}, $L_{0.5-2keV} \sim 10^{39}$ erg s^{-1}). Moreover, we performed ChaRT[8] and MARX[9] simulations of the strong nuclear source and the resolved extended emission using *Chandra* ACIS spectra(Yang et al. 2001; Wang et al. 2010), which demonstrate that the point spread function (PSF) wings of the nuclear emission and the extended emission can only contribute

[8] See `http://cxc.harvard.edu/chart/`
[9] Version 4.3; See `http://space.mit.edu/cxc/marx/`

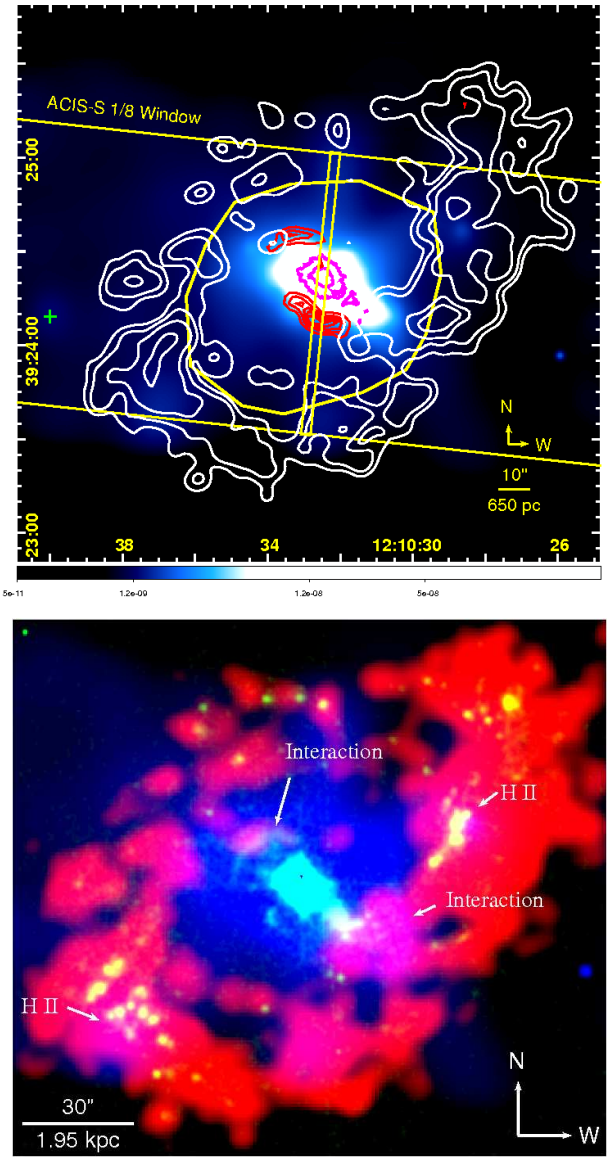

FIG. 1.— (a) Exposure corrected, adaptively smoothed ACIS image (0.3–1 keV) of NGC 4151, overlaid with the HI emission in contours. Yellow polygon outlines the spectral extraction region. Magenta contours indicate the spatial extent of the optical ENLR (Kaiser et al. 2000). Red contours represent the ^{12}CO line emission (Dumas et al. 2010). A faint X-ray enhancement at $r = 80''$ is marked with a cross. (b) Three-color composite image of the central $3' \times 3'$ region. Red represents the HI λ21 cm emission (Mundell & Shone 1999), green the continuum-subtracted Hα emission (Knapen et al. 2004), and blue the soft X-ray emission. Magenta (X-ray+HI) represents X-ray emission associated with the outflow/ISM interaction region and HII regions. Note that green (Hα) mostly appears as yellow (Hα+HI) and cyan (Hα+X-ray), which highlights the HII regions and the ionized bicone, respectively.

157±12 counts and 42±6 counts in the 0.3–1 keV band in the extraction region, respectively.

We extracted the ACIS spectrum of the soft X-ray emission in the same region. The background subtracted X-ray spectrum is poorly fitted with an absorbed power-law model that is consistent with the nuclear spectrum ($\Gamma = 1.68$; Wang et al. 2010), showing significant line emission residuals in the 0.3–1 keV range. Moreover, the spectrum can be neither fitted by a single photoionized

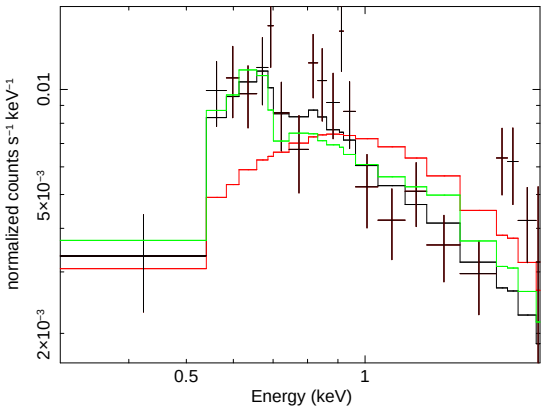

FIG. 2.— Spectral fits to NGC 4151's extended emission (0.3–2 keV), using a power-law component (red), a thermal plasma model (black), and a photoionization model (green). The absorption is fixed at the line-of-sight Galactic column $N_H = 2 \times 10^{20}$ cm^{-2}.

emission model (*photemis*; see XSTAR[10]) nor a thermal plasma (APEC; Smith et al. 2001) model (χ^2/dof = 182/83 and 178/83, respectively).

The fit is much improved when a power-law component with a photoionized emission component is used ($\log\xi = 1.7 \pm 0.2$), where ionization parameter $\xi \equiv L/nR^2$ (Kallman & McCray 1982). The fit is slightly improved when a thermal plasma (APEC; Smith et al. 2001) component ($kT = 0.25^{+0.04}_{-0.03}$ keV) is adopted. In both two-component fits, the power-law component contributes ∼50% of the 0.3–2 keV flux. The results are summarized in Table 1.

The surface brightness profile of the extended emission is shown in Figure 3, using $\Delta r = 5''$ concentric annuli starting at $r = 15''$ from the nucleus. The small excess at $r \sim 160$ pixel ($80''$) is due to a faint extended ($d \sim 6''$) X-ray enhancement ($L_x \sim 4 \times 10^{37}$ ergs s^{-1} assuming the same $kT \sim 0.25$ keV) centered at α=$12^h10^m39.^s9$, δ=+39°24′10″ (P.A.∼120°). It appears to be spatially coincident with the faint diffuse HI gas seen around the outer ends of the bar connecting to the spiral arms (Pedlar et al. 1992).

4. DISCUSSION

4.1. *Nature of the Soft X-ray Emission*

We consider four hypotheses for the extended soft X-rays on spatial scales of $\sim 10^4$ light year:

1. Unresolved Point Sources–Active star formation in the region of the HI cavity is at a low level, as indicated by the lack of Hα emission and weak PAH emission (Asif et al. 2005). Adopting the empirical measured $L_x/M_* \sim 8.2 \times 10^{27}$ erg s^{-1} M$_\odot^{-1}$ (Revnivtsev et al. 2008) and a bulge mass of $M_* \sim 10^9 M_\odot$ for NGC 4151 (Wandel 2002), the expected combined contribution of the unresolved old stellar population (low mass X-ray binaries and cataclysmic variables) is $L_{0.5-2keV} \sim 10^{37}$ erg s^{-1}, two orders of magnitude lower than the detected soft emission ($L_{0.5-2keV} \sim 10^{39}$ erg s^{-1}). Moreover, the K-band starlight profile (Knapen et al. 2003) decreases faster than the X-ray emission profile (Figure 3). Thus we conclude that the contribution of stellar sources is negligible.

2. Electron Scattered Nuclear Emission–The hot plasma around the nucleus could electron scatter a fraction of the nuclear flux at a larger radii (e.g., NGC 1068, Elvis et al. 1990). Assuming a solid angle $\Omega = 4\pi$ for a scattering medium, the observed $L_x/L_{x,nuc}$ implies an electron scattering optical depth of $\tau_{es} = 0.01$ and a mean column density of $N_H \sim 10^{22}$ cm^{-2}. Adopting 200 pc for the depth, the typical galactic disk scale height (e.g., Padoan et al. 2001), this corresponds to a volume density of $n_e \sim 15$ cm^{-3}. This is ∼100 times higher than n_e inferred for the thermal plasma and so thermal emission (which scales as n_e^2) will dominate the emission unless it is much cooler than 10^6 K. The scattering medium must also be highly ionized, requiring $T \gtrsim 3 \times 10^6$ K if this is achieved thermally. For the electron-scattering model to be self-consistent, a photoionized medium (eliminating T discrepancy) or a historic outburst ($\sim 10^4$ yr ago) during which the nucleus was 100 times brighter than currently observed (eliminating n_e discrepancy) is needed.

However, the poor fit with the nuclear power-law model (§ 3.2) does not support this scenario. Moreover, the required power-law component in either two-component fits ($L_{0.5-2keV} \sim 4 \times 10^{38}$ erg s^{-1}) is comparable to the expected total contribution ($L_{0.5-2keV} \sim 2.5 \times 10^{38}$ erg s^{-1}) from PSF scattering and unresolved point sources, which allows little contribution from the electron scattered component. We conclude that an electron scattered component is not important for the extended emission.

3. Photoionized Gas–The faint extended emission in NGC 4151 could be due to gas photoionized by a more luminous AGN in the past. Such a "quasar-relic" scenario was proposed for NGC 5252, which has a spectacular ionization cone extending ∼10 kpc from the nucleus (Dadina et al. 2010). Observable signatures of such "afterglow" from an outburst in a radio quiet quasar ($L \sim 10^{46}$ erg s^{-1}) have been studied by Wang et al. (2005). In this context, NGC 4151 belongs to the regime of the lower luminosity sources, for which Wang et al. (2005) suggest an X-ray spectrum dominated by Lyα and Lyβ lines of NeX and OVIII. Under this assumption, the $0.3-1$ keV emission is dominated by line emission blended at ACIS' spectral resolution, which in turn implies an ionization parameter of $\log\xi \sim 1.6-2.1$(Kallman & McCray 1982; Yang et al. 2001) consistent with $\log\xi = 1.7$ measured in XSTAR. Adopting an electron density $n = 2$ cm^{-3} (equal to the HI density) and $R = 3$ kpc, the required ionizing luminosity of the nucleus is $L_{ion} \sim 6 \times 10^{45}$ erg s^{-1} $\sim L_{Edd}$ ($M_{BH} = 4 \times 10^7 M_\odot$; Bentz et al. 2006). Based on detailed photoionization modeling of the extended optical emission of NGC 4151 (Schulz & Komossa 1993), the photoionizing continuum could be anisotropic and the ionizing flux towards the ENLR may be ∼10 times higher than that in the direction of the earth. This is still insufficient to power the more extended X-ray emission. Therefore an Eddington-limit outburst of NGC 4151 $\sim 10^4$ yr in the past is required.

The same photoionized medium would produce [OIII] emission. If we adopt an observed [OIII]/soft X-ray ratio of ∼10 for $\log\xi \sim 1.7$ photoionized gas (Bianchi et al.

[10] Version 2.2; available at `http://heasarc.nasa.gov/docs/software/xstar/xstar.html`

TABLE 1
Spectral Fit of the NGC 4151 Extended Emission

Model[a]	χ^2/dof	Parameter	$F_{0.5-2keV}$[b]
Electron Scattering (*pow*)	104/83	$\Gamma = 1.68$	3.0
Photoionization (*photemis* + *pow*)	78/82	$\log\xi = 1.7 \pm 0.2$	3.2
Thermal Plasma (*apec* + *pow*)	73/82	$kT = 0.25^{+0.04}_{-0.03}$	3.2

[a] A fixed line-of-sight $N_H = 2 \times 10^{22}$ cm^{-2} (Murphy et al. 1996) is adopted for all fits using the 0.3–2 keV spectrum.
[b] In unit of 10^{-14} erg s^{-1} cm^{-2}.

2006), the expected [OIII] surface brightness is $\sim 10^{-16}$ erg s^{-1} cm^{-2} arcsec^{-2}, fainter than the sensitivity limit of existing [OIII] images (e.g., $F_{lim} \sim 10^{-15} - 10^{-16}$ erg s^{-1} cm^{-2} arcsec^{-2}; Pérez-Fournon & Wilson 1990; Evans et al. 1993; Kaiser et al. 2000). Thus a photoionized origin is still open to direct testing.

4. Confined Hot Gas–We model the background subtracted surface brightness profile with a 1-d β model provided in SHERPA[11] ($\Sigma_x \propto [1+(r/r_0)^2]^{-3\beta+1/2}$, where r_0 is the core radius). This model is often adopted in studies of the hot gas in early type galaxies (e.g., Trinchieri et al. 1986). The best-fit index is $\beta = 0.39^{+0.03}_{-0.02}$, implying a brightness profile that is decreasing slower than an adiabatically expanding wind ($\Sigma_x \propto r^{-3}$), and confinement of the hot gas. We attempted fitting spectra extracted from two concentric annuli at radii $\Delta r = 15'' - 30''$ and $30'' - 45''$. Within the uncertainties, the thermal fits give the same temperature ($kT = 0.25 \pm 0.07$ keV and $kT = 0.22^{+0.05}_{-0.03}$ keV), implying that any hot gas is approximately isothermal.

Under this assumption, we derived the pressure radial profile of the hot gas based on the surface brightness profile, considering two cases for the volume in which the hot gas is contained: a cyclinder or a sphere. For the cylinder, we assumed a depth of 200 pc. To calculate the volume emission density of spherically symmetric gas, we account for the projection effect by successively subtracting outer shells to smaller radii (Kriss et al. 1983). The electron density distribution is then derived from the emission per unit volume, adopting the simple approximation $\epsilon \approx 6.2 \times 10^{-19} T^{-0.6} n_p^2$ erg s^{-1} cm^{-3} (McKee & Cowie 1977) for the emissivity of a $kT = 0.25$ keV thermal gas (§ 3.2).

The pressure of the X-ray gas gradually decreases from 10^{-11} to approximately $\sim 5 \times 10^{-12}$ dyne cm^{-2} when reaching the HI gas lanes. Without confinement, the gas will inevitably expand, cooling too much to be observed in the X-rays. We estimate that the thermal pressure of CO is $\sim 10^{-15}$ dyne cm^{-2}, using the mass measured in Dumas et al. (2010), thus the molecular gas present ($T \sim 10$ K) cannot provide the pressure balance. The estimated thermal pressure of the HI material is $\sim 2 \times 10^{-12}$ dyne cm^{-2}, assuming $T \sim 8000$ K[12] and a column density $N_H = 1.5 \times 10^{21}$ cm^{-2} (Mundell et al. 1999). This is well matched to the pressure required to provide the confinement needed to prevent the hot gas from expanding in the disk plane where atomic gas is most dense.

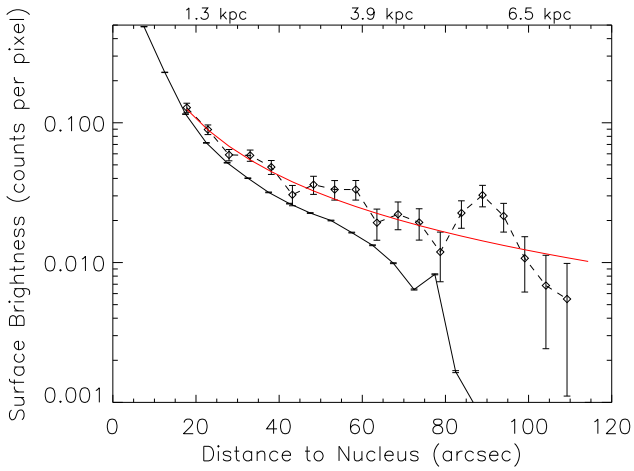

Fig. 3.— NGC 4151 surface brightness profile (background subtracted; dashed line) derived from ACIS 0.3–1 keV image. The red line shows the best fit with a 1-d β model. The solid black line represents the K-band surface brightness profile from Knapen et al. (2003), resembling the integrated distribution of star light in NGC 4151's bulge.

Mundell et al. (1999) showed that the isovelocity contours of the HI emission deviate from a circularly rotating disk, and identified kinematic evidence for the presence of shocks in inflowing gas along the stellar bar. Taking an average inflow velocity of v$\sim$40 km s^{-1} (Mundell et al. 1999) and a particle density of $n = 2$ cm^{-3} in the HI gas lanes, the dynamic pressure as a result of the inflowing motion, is $\rho v^2 \sim 10^{-11}$ dyne cm^{-2}, where $\rho = nm_p$ is the density. This provides additional pressure for the neutral material to be in equilibrium with the hot gas.

4.2. *Implications on the Timescale of AGN-host Interaction*

The presence of soft X-ray emission (either thermal or photoionized) on a $\gtrsim$2 kpc scale is interesting. If the X-ray emission originates from hot gas heated by the AGN outflow, it would be strong evidence for AGN feedback to the ISM on galaxy-scales, resembling the larger scale AGN feedback from radio bubbles interacting with the intracluster medium seen in the Perseus cluster (Fabian et al. 2003).

In the photoionized scenario, considering the light travel time from the nucleus to the HI gas lanes (10^4 yr) and the photoionization recombination timescale $t_{rec} \approx 200(n/10^9)^{-1}(T/10^5)^{0.7}$ s ($\sim 1.5 \times 10^4$ yr under the above assumptions; Reynolds 1997), we can constrain

[11] http://cxc.harvard.edu/sherpa/
[12] This value is adopted from measurements in our galaxy, considering turbulence over the galaxy and typical disk line widths (e.g., Sellwood & Balbus 1999). Note that the average brightness temperature of HI in our galaxy is $T \sim 100 - 150$ K (Clark 1965).

the timescale when NGC 4151 was experiencing such an Eddington-limit outburst phase to be $t_{Edd} < 2.5 \times 10^4$ yr ago. Otherwise the X-ray gas would no longer emit recombination lines.

If the soft diffuse emission is due to shock heating associated with a nuclear outflow instead, the current $L_{bol} = 7.3 \times 10^{43}$ (Kaspi et al. 2005) indicates $L_{bol}/L_{Edd} \sim 0.01$. Assuming that $\sim 5\%$ of the power has gone to create the HI cavity (e.g., Silk & Rees 1998; Hopkins et al. 2005), $\sim 4 \times 10^4$ year of such AGN heating is needed to produce the thermal energy content of the hot gas ($E_{th} \sim 3 \times 10^{54}$ erg). This is much shorter than the current cooling time of the hot gas ($\tau_c \sim 10^8$ yr). The efficiency at which the AGN outflow deposits its kinematic energy in the ISM can be as low as 10^{-4}, provided that the hot gas is confined and the duration of the strong nuclear outflow is $\tau_{outflow} \ll \tau_c$.

However, perpendicular to the plane, the gas could expand and cool efficiently via adiabatic expansion unless some other confinement exists. Assuming an outflow velocity of $v_{outflow} \sim 10^3$ km s^{-1} (typical of the NLR clouds; Kaiser et al. 2000) for the free expansion perpendicular to the disk (c.f. thermal velocity dispersion $v_{th} = \sqrt{k_B T/m_p} \sim 100$ km s^{-1}), the relevant timescale is the time span in which the hot gas expands to the scale height above disk plane $\Delta R/v_{outflow} \sim 10^5$ yr. This timescale again implies that the timescale to the last AGN outflow heating must be $< 10^5$ yr, in order to replenish the X-ray gas expanding out of the plane that is cooling rapidly.

Compared to the estimated AGN lifetime ($10^7 - 10^8$ yrs), the fact that we observe the AGN-host interaction is intriguing given the short timescale to the last episode of activity. Such episodic outbursts must occur frequently (Ciotti et al. 2010), and our finding implies they may occupy $\gtrsim$1% of the AGN lifetime.

5. CONCLUSIONS

To summarize, we have discovered soft (0.3–1 keV) diffuse X-ray emission ($L_{0.5-2keV} \sim 10^{39}$ erg s^{-1}) in the central $\sim$2 kpc of NGC 4151, which cannot be attributed to PSF scattering or electron scattering of the nuclear emission, or the integrated emission from unresolved faint point sources.

If the gas is of photoionized origin and represents the relic of past AGN activities, the nucleus of NGC 4151 must have experienced an Eddington-limited high luminosity phase. Alternatively, AGN outflows may have mechanically heated the gas to X-ray emitting temperature ($kT = 0.25$ keV). This hot gas could be confined in the HI cavity by the thermal pressure of the HI gas and dynamic pressure of infalling gas along the large-scale stellar bar.

For both scenarios, the AGN-host interaction must have occured relatively recently. For the AGN outflow heating to work, the deposit of mechanical energy must have happened $\lesssim 10^5$ yr ago to replenish the hot gas, which is expanding out of the plane unless prevented by other confining mechanism. Whereas for photoionized gas from a past AGN outburst, the timescale to the highly active phase must be $\lesssim 2.5 \times 10^4$ yr ago. This short timescale to the last episode of high activity phase may imply such outbursts occupy $\gtrsim$1% of the AGN lifetime.

We thank the anonymous referee for helpful comments. This work is partially supported from NASA grant GO8-9101X and NASA Contract NAS8-39073 (CXC). GD acknowledges support from DFG grants SCH 536/4-1 and SCH 536/4-2 as part of the SPP 1177.

REFERENCES

Asif, M. W., Mundell, C. G., Pedlar, A., Unger, S. W., Robinson, A., Vila-Vilaro, B., & Lewis, J. R. 1998, A&A, 333, 466
Asif, M. W., Mundell, C. G., & Pedlar, A. 2005, MNRAS, 359, 408
Bianchi, S., Guainazzi, M., & Chiaberge, M. 2006, A&A, 448, 499
Bentz, M. C., et al. 2006, ApJ, 651, 775
Ciotti, L., Ostriker, J. P., & Proga, D. 2010, ApJ in press, arXiv:1003.0578
Clark, B. G. 1965, ApJ, 142, 1398
Das, V., et al. 2005, AJ, 130, 945
Dadina, M., Guainazzi, M., Cappi, M., Bianchi, S., Vignali, C., Malaguti, G., & Comastri, A. 2010, A&A, in press, arXiv:1003.1665
Dumas, G., Schinnerer, E., & Mundell, C. G. 2010, ApJ, in press
Elvis, M., Briel, U. G., & Henry, J. P. 1983, ApJ, 268, 105
Elvis, M., Fassnacht, C., Wilson, A. S., & Briel, U. 1990, ApJ, 361, 459
Evans, I. N., Tsvetanov, Z., Kriss, G. A., Ford, H. C., Caganoff, S., & Koratkar, A. P. 1993, ApJ, 417, 82
Fabian, A. C., Sanders, J. S., Allen, S. W., Crawford, C. S., Iwasawa, K., Johnstone, R. M., Schmidt, R. W., & Taylor, G. B. 2003, MNRAS, 344, L43
Freeman, P. E., Kashyap, V., Rosner, R., & Lamb, D. Q. 2002, ApJS, 138, 185
González-Martín, O., 2008, PhD Thesis, Instituto de Astrofísica de Andalucía, Granada, Spain
Hopkins, P. F., Hernquist, L., Cox, T. J., Di Matteo, T., Martini, P., Robertson, B., & Springel, V. 2005, ApJ, 630, 705
Hopkins, P. F., & Elvis, M. 2010, MNRAS, 401, 7
Kaiser, M. E., et al. 2000, ApJ, 528, 260
Kallman, T. R., & McCray, R. 1982, ApJS, 50, 263
Kaspi, S., Maoz, D., Netzer, H., Peterson, B. M., Vestergaard, M., & Jannuzi, B. T. 2005, ApJ, 629, 61
Knapen, J. H., de Jong, R. S., Stedman, S., & Bramich, D. M. 2003, MNRAS, 344, 527
Knapen, J. H., Stedman, S., Bramich, D. M., Folkes, S. L., & Bradley, T. R. 2004, A&A, 426, 1135
Kraemer, S. B., Schmitt, H. R., & Crenshaw, D. M. 2008, ApJ, 679, 1128
Kriss, G. A., Cioffi, D. F., & Canizares, C. R. 1983, ApJ, 272, 439
McKee, C. F., & Cowie, L. L. 1977, ApJ, 215, 213
Mundell, C. G., Pedlar, A., Baum, S. A., O'Dea, C. P., Gallimore, J. F., & Brinks, E. 1995, MNRAS, 272, 355
Mundell, C. G., & Shone, D. L. 1999, MNRAS, 304, 475
Mundell, C. G., Pedlar, A., Shone, D. L., & Robinson, A. 1999, MNRAS, 304, 481
Mundell, C. G., Wrobel, J. M., Pedlar, A., & Gallimore, J. F. 2003, ApJ, 583, 192
Murphy, E. M., Lockman, F. J., Laor, A., & Elvis, M. 1996, ApJS, 105, 369
Ogle, P. M., Marshall, H. L., Lee, J. C., & Canizares, C. R. 2000, ApJ, 545, L81
Ostriker, J. P., Choi, E., Ciotti, L., Novak, G. S., & Proga, D. 2010, arXiv:1004.2923
Padoan, P., Kim, S., Goodman, A., & Staveley-Smith, L. 2001, ApJ, 555, L33
Pedlar, A., Howley, P., Axon, D. J., & Unger, S. W. 1992, MNRAS, 259, 369
Pérez-Fournon, I., & Wilson, A. S. 1990, ApJ, 356, 456
Revnivtsev, M., Churazov, E., Sazonov, S., Forman, W., & Jones, C. 2008, A&A, 490, 37
Reynolds, C. S. 1997, MNRAS, 286, 513
Schulz, H., & Komossa, S. 1993, A&A, 278, 29

Sellwood, J. A., & Balbus, S. A. 1999, ApJ, 511, 660
Silk, J., & Rees, M. J. 1998, A&A, 331, L1
Smith, R. K., Brickhouse, N. S., Liedahl, D. A., & Raymond, J. C. 2001, ApJ, 556, L91
Storchi-Bergmann, T., McGregor, P. J., Riffel, R. A., Simões Lopes, R., Beck, T., & Dopita, M. 2009, MNRAS, 394, 1148
Storchi-Bergmann, T., Lopes, R. D. S., McGregor, P. J., Riffel, R. A., Beck, T., & Martini, P. 2010, MNRAS, 402, 819
Trinchieri, G., Fabbiano, G., & Canizares, C. R. 1986, ApJ, 310, 637
Ulrich, M.-H. 2000, A&A Rev., 10, 135
Wandel, A. 2002, ApJ, 565, 762
Wang, J.-M., Yuan, Y.-F., & Ho, L. C. 2005, ApJ, 625, L5
Wang, J., Fabbiano, G., Karovska, M., Elvis, M., Risaliti, G., Zezas, A., & Mundell, C. G. 2009, ApJ, 704, 1195
Wang, J., Risaliti, G., Fabbiano, G., Elvis, M., Zezas, A., & Karovska, M. 2010, ApJ, 714, 1497
Yang, Y., Wilson, A. S., & Ferruit, P. 2001, ApJ, 563, 124